1-1-2020

Estimating corn emergence date using UAV-based imagery

Chin Nee Vong
University of Missouri

Stirling A. Stewart
University of Missouri

Jianfeng Zhou
University of Missouri, zhoujianf@missouri.edu

Newell R. Kitchen
USDA Agricultural Research Service

Kenneth A. Sudduth
USDA Agricultural Research Service

ESTIMATION OF CORN EMERGENCE DATE USING UAV IMAGERY

Chin Nee Vong[1], Stirling A. Stewart[2], Jianfeng Zhou[1,*], Newell R. Kitchen[3], Kenneth A. Sudduth[3]

[1] Division of Food Systems and Bioengineering, University of Missouri, Columbia, Missouri, USA.
[2] Division of Plant Sciences, University of Missouri, Columbia, Missouri, USA.
[3] USDA-ARS Cropping Systems and Water Quality Research Unit, Columbia, Missouri, USA.
[*] Correspondence: zhoujianf@missouri.edu.

HIGHLIGHTS

- UAV imagery can be used to characterize newly-emerged corn plants.
- Size and shape features used in a random forest model are able to predict days after emergence within a 3-day window.
- Diameter and area were important size features for predicting DAE for the first, second, and third week of emergence.

ABSTRACT. *Assessing corn (*Zea mays *L.) emergence uniformity soon after planting is important for relating to grain production and making replanting decisions. Unmanned aerial vehicle (UAV) imagery has been used for determining corn densities at vegetative growth stage 2 (V2) and later, but not as a tool for quantifying emergence date. The objective of this study was to estimate days after corn emergence (DAE) using UAV imagery and a machine learning method. A field experiment was designed with four planting depths to obtain a range of corn emergence dates. UAV imagery was collected during the first, second, and third weeks after emergence. Acquisition height was approximately 5 m above ground level, which resulted in a ground sampling distance of 1.5 mm pixel^{-1}. Seedling size and shape features derived from UAV imagery were used for DAE classification based on a random forest machine learning model. Results showed that 1-day DAE could be distinguished based on image features within the first week after initial corn emergence with a moderate overall classification accuracy of 0.49. However, for the second week and beyond, the overall classification accuracy diminished (0.20 to 0.35). When estimating DAE within a 3-day window (-1 to +1 day), the overall 3-day classification accuracies ranged from 0.54 to 0.88. Diameter, area, and the ratio of major axis length to area were important image features to predict corn DAE. Findings demonstrated that UAV imagery can detect newly-emerged corn plants and estimate their emergence date to assist in assessing emergence uniformity. Additional studies are needed for fine-tuning the image collection procedures and image feature identification to improve accuracy.*

Keywords. *Corn emergence, Image features, Random forest, Unmanned aerial vehicle.*

Corn is one of the most important food crops in the world as well as a vital source for animal feed and biofuel (Klopfenstein et al., 2013; Shiferaw et al., 2011). Based on the latest report from the Food and Agriculture Organization of the United Nations (FAO, 2020), total global corn (maize) production in 2018 was more than 1.1 billion tons, with a harvested area of close to 200 million ha. To maximize corn grain yield, management is needed to optimize seedling emergence uniformity (i.e., emergence time) and seedling spatial uniformity (i.e., plant spacing). Temporal variation in seedling emergence leads to consistent yield reductions (Andrade and Abbate, 2005; Liu et al., 2004; Nafziger et al., 1991). Nafziger et al. (1991) showed that the average harvested yield of corn decreased by 6% and 12% when planting was delayed 10 to 12 days and 22 days, respectively. Meanwhile, Liu et al. (2004) found that the average yield decreased by 4.3% and 8.7% with planting delays of 12 and 21 days, respectively. In a separate study, the average yield of corn with an emergence difference of three days was about 12% less than that of the corn in control plots with uniform emergence (Andrade and Abbate, 2005).

Evaluating the temporal variation in seedling emergence is also necessary for making replanting decisions, by assessing the effect of the variation in both the time of emergence and the proportion of delayed plants on final grain yield (Nafziger et al., 1991). As stated by Lauer (1997), the first step in making replanting decisions is crop scouting at multiple regions of the field to determine the plant population and its uniformity. However, this method is labor-intensive, subjective, and spatially inadequate for fields with variable soil conditions that influence seed germination and

Submitted for review on 8 June 2020 as manuscript number ITSC 14145; approved for publication as a Research Article by the Information Technology, Sensors, & Control Systems Community of ASABE on 18 March 2021.

Mention of company or trade names is for description only and does not imply endorsement by the USDA. The USDA is an equal opportunity provider and employer.

emergence. With the advantages of unmanned aerial vehicles (UAV), optical sensors, advanced image processing, and analytic technologies, the time and labor needed for crop scouting can be greatly reduced (Shuai et al., 2019), and a more precise and accurate estimation of plant density can be acquired.

Research has shown the usefulness of UAV red-green-blue (RGB) imagery in determining corn plant density and spacing estimation at early stages. Gnädinger and Schmidhalter (2017) used aerial images to determine corn post-emergence plant density at vegetative growth stages V3 to V5 (i.e., three to five visible leaves; Ransom et al., 2020) and achieved an accuracy of $R^2 = 0.89$. Varela et al. (2018) demonstrated the potential of using high-resolution RGB images with a spatial resolution of 2.4 mm pixel^{-1} to estimate corn stand count at the V2 to V3 growth stages based on supervised learning techniques. In addition, UAV imagery was used to estimate corn plant spacing (Zhang et al., 2018) and corn plant density at about two weeks after emergence (Shuai et al., 2019). The results from Shuai et al. (2019) showed precision of at least 96% when estimating the number of plants and R^2 of 0.89 to 0.91 when estimating the plant spacing. All these studies showed promising results for using UAV imagery in detecting and counting corn seedlings as well as estimating plant spacing. However, none of them used UAV imagery for detecting corn emergence at much earlier stages (i.e., pre-growth stage V2) and quantifying emergence date of seedlings.

Previous research has also used UAV-derived image features, including size and shape (e.g., area, diameter, major axis length, minor axis length, solidity, and eccentricity) to estimate wheat density (Jin et al., 2017) and detect corn at an early growth stage (Varela et al., 2018). Jin et al. (2017) used these features in a support vector machine to estimate the wheat density and achieved R^2 values from 0.80 to 0.91 at different experiment sites. Varela et al. (2018) used image features in a decision tree to classify corn and non-corn objects (weeds) and found that aspect ratio, axis-diameter ratio, convex area, thinness, and solidity were significant image features in the classification. In addition, the size and shape used in artificial neural network modeling were effective image features for distinguishing different varieties of corn seed (accuracy of 0.88 to 0.92, Chen et al., 2010) and rice seed (accuracy of 0.70 to 0.95, Chaugule and Mali, 2014).

Our review of the literature did not reveal any previous research on determining plant emergence date based on image features. Because corn emerges across a range of days, early and late emerging seedlings have different size and shape characteristics. These characteristics could be identified using image features and would be useful in classifying the number of days after emergence (DAE) for each individual plant seedling. The overall objective of this study was to estimate the DAE using size and shape features extracted from UAV imagery. Specific objectives were (1) to extract size and shape features from corn plant images, (2) to build a random forest (RF) machine learning model to predict corn plant DAE, and (3) to identify important image features in predicting plant DAE.

Materials and Methods

Experimental Site and Setup

The experiment was conducted at the Bay Farm Research Facility of the University of Missouri, Columbia, Missouri (38° 52′ 45.3″ N, 92° 12′ 15.3″ W) with 18 plots arranged in a randomized complete block design, as shown in figure 1a. Treatments included four planting depths (3.8, 5.1, 6.4, and 7.6 cm) with four replications (with an additional replication for the 5.1 and 7.6 cm depths). This range of depths produced variability in corn emergence date. Each plot was 3.0 m long and included four rows of corn with an inter-row spacing of 0.76 m and average intra-row spacing of 17.7 cm. Only the middle two rows were selected for manual measurement and image analysis, as shown in figure 1b. All corn was planted on 9 April 2019 with no-till using a custom-built John Deere four-row planter that was equipped with MaxEmerge XP row units (Deere & Co., Moline, Ill.) adjusted to plant seeds at the four defined depths. Corn emergence was checked daily beginning on 22 April (first emergence) until complete emergence (29 April), with newly-emerged plants marked with unique color stakes for each day. Emergence was not checked on 28 April due to time constraint, and the plants that emerged on 29 April.

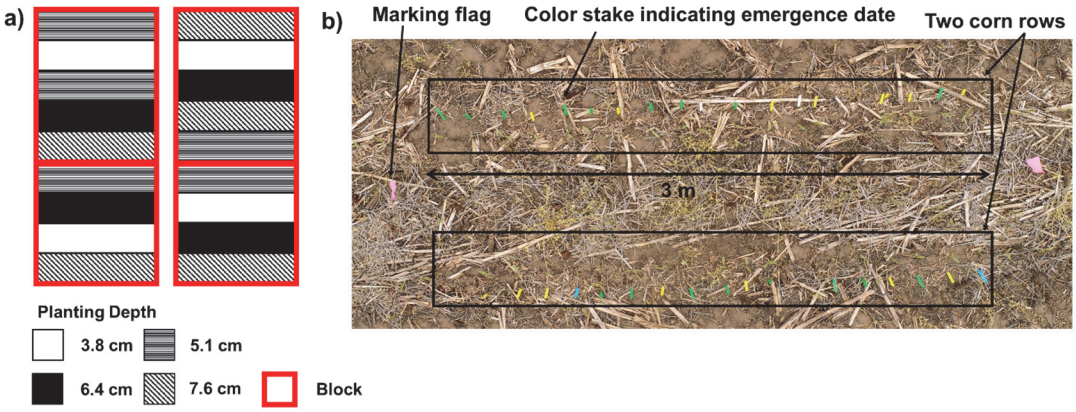

Figure 1. (a) Schematic of plots arranged in randomized complete block design and (b) example UAV image of a study plot captured at about 5 m height on 3 May 2019 (DAE 5 to 12).

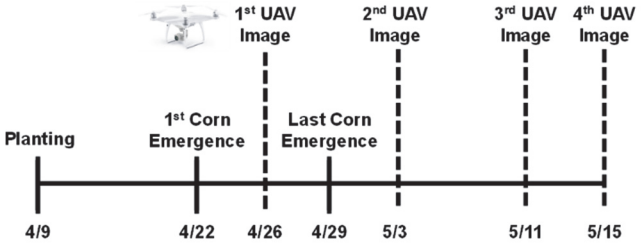

Figure 2. Corn emergence dates and UAV image collection dates.

UAV Image Collection

Aerial images were collected using a Phantom 4 Advanced UAV imaging system (DJI, Shenzhen, Guangdong, China) with an onboard camera that has a field-of-view (FOV) of 84° and an image size of 4864 × 3648 pixels (20M pixels). The DJI Go 4 app was used to set the UAV height at 5 m above ground level (AGL), resulting a ground sampling distance (GSD) of 1.5 mm pixel^{-1}. The GSD is the distance between two consecutive pixel centers measured on the ground (Orych, 2015). The camera was adjusted to vertically face down toward the field, i.e., nadir view (Lillesand et al., 2004), to acquire images of each plot. The images were taken manually using the default camera settings (auto white balance and ISO range). Aerial image data were collected on 26 April and on 3, 11, and 15 May. The aerial images collected on 26 April were to test the capability of the UAV images to detect corn within the first week after first emergence (DAE 1 to 5 in this study). The aerial images collected on later dates represented 5 to 12, 13 to 20, and 17 to 24 days after first emergence. Figure 2 summarizes the timeline of corn emergence and the dates of aerial image collection.

Image Processing and Feature Extraction

Small corn seedlings from DAE 1 to 5 were difficult to identify due to their small size. Additionally, identifying seedlings was particularly difficult at the no-till research site because abundant ground residue and patches of winter annual weeds obscured the seedlings (fig. 1b). Therefore, each corn seedling was manually cropped from the UAV images to simplify the image processing procedure. To identify corn seedlings in the images, a contrast enhancement procedure based on linear contrast stretch was performed on each image using the *decorrstretch* function in MATLAB (R2017b, MathWorks, Natick, Mass.) (Gnädinger and Schmidhalter, 2017). Linear contrast stretch expands the original pixel values in the image linearly into a new distribution (Chandpa et al., 2014). The *decorrstretch* function in MATLAB transforms the pixel values of each band into the color eigenspace of a 3 × 3 (three bands of R, G, and B) correlation matrix, followed by stretching them to equalize the band variances and transforming the color range to a normalized interval between 0.01 and 0.99 (using the "Tol" and "0.01" arguments in the *decorrstretch* function). This function enhanced the color differences between corn seedlings and the background (soil or residue) (fig. 3) to segment the corn seedlings accurately. The contrast-enhanced images in RGB color space were converted to HSV (hue, saturation, value) color space to eliminate the luminance effect. The Color Thresholder app in MATLAB was used to determine the threshold value for each band in HSV color space to segment the images (fig. 3).

Size and shape features were then extracted using the *regionprops* function in MATLAB or computed using the equations listed in table 1. The actual values (in mm or mm^2) of the calculated image features listed in table 1 were computed using the product of the number of pixels of the stated image features and the GSD. The GSD of each image was determined using reference boards with known dimensions and the length of color stakes in each UAV image. This GSD determination is useful to show the needed GSD ranges for detecting the small newly-emerged plants.

Random Forest Machine Learning Model

A random forest (RF) modeling method was used to predict corn plant DAE. The RF model is a type of classification and regression tree (CART) machine learning method employing ensembles of classifications (James et al., 2013; Rodriguez-Galiano et al., 2012). Advantages offered by an RF model include fast training, higher accuracy, less potential for overfitting (when using a large number of trees), measures of variable importance, ability to capture non-linear correlations between variables and predictors, and no requirement for data distribution assumptions such as normality (Belgiu and Drăguţ, 2016; James et al., 2013; O'Brien

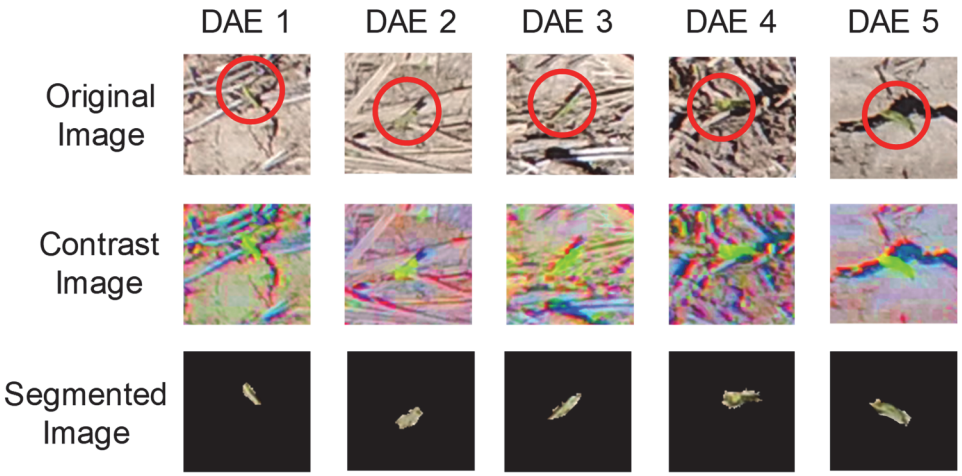

Figure 3. Segmented corn images at different DAE using contrast enhancement and segmentation with threshold values from HSV color space.

Table 1. Size and shape features (SF1 to SF7) extracted from each corn image.

Feature	Description or Equation	Reference
Area	Total pixel number of a segmented seedling in images.	MATLAB[a]
Perimeter	Pixel number around the boundary of a segmented seedling.	MATLAB[a]
Diameter	Pixel number of the diameter of an equivalent circle with the same area as the segmented seedling.	MATLAB[a]
Major axis length	Pixel number of the major axis of an equivalent ellipse of the segmented seedling.	MATLAB[a]
Minor axis length	Pixel number of the minor axis of an equivalent ellipse of the segmented seedling.	MATLAB[a]
Eccentricity	Ratio of the distance between the foci of the ellipse and its major axis length (ellipse with eccentricity 0 is a circle and 1 is a line segment).	MATLAB[a]
Solidity	Proportion of pixels in the convex hull that are also in the region.	MATLAB[a]
Aspect ratio	$\frac{\text{Major axis length}}{\text{Minor axis length}}$	Najafabadi and Farahani, 2012
Roundness	$\frac{4\pi \times \text{Area}}{\text{Perimeter}}$	Najafabadi and Farahani, 2012
Compactness	$\frac{\text{Perimeter}^2}{\text{Area}}$	Najafabadi and Farahani, 2012
SF1	$\frac{1}{\text{Compactness}}$	Changule and Mali, 2014
SF2	$\frac{\text{Major axis length}}{\text{Area}}$	Changule and Mali, 2014
SF3	$\frac{\text{Area}}{\text{Major axis length}^3}$	Changule and Mali, 2014
SF4	$\frac{\text{Area}}{\left(\frac{\text{Major axis length}}{2}\right)^2 \times \pi}$	Changule and Mali, 2014
SF5	$\frac{\text{Area}}{\frac{\text{Major axis length}}{2} \times \frac{\text{Minor axis length}}{2} \times \pi}$	Changule and Mali, 2014
SF6	$\frac{\text{Minor axis length}}{\text{Area}}$	
SF7	$\frac{\text{Area}}{\text{Minor axis length}^3}$	

[a] Image features extracted using the *regionprops* function in MATLAB (R2017b).

and Ishwaran, 2019; Rodriguez-Galiano et al., 2012). To develop the RF model, a dataset consisting of the response variable (DAE) and 17 image features (table 1) was established with 70% of the images as training data and 30% of the images as testing data. The number of observations was 310 for 26 April, 627 for 3 May, and 624 for both 11 and 15 May. For every tree branch built in the RF model, only four features were randomly selected, instead of using the full set of features to decorrelate the trees and build a reliable model (James et al., 2013). Because an RF model does not overfit even when using a large number of trees, studies have suggested that the ideal number of trees ranges from 64 to 500 (Belgiu and Drăguţ, 2016; James et al., 2013; Oshiro et al., 2012). In this study, open-source software (RStudio ver. 1.2.1335, RStudio, Boston, Mass.) was used for conducting RF modeling using the *randomForest* package (Breiman and Cutler, 2018). The default value of 500 trees in the package was used.

The model performance was evaluated using the test data with two metrics, i.e., accuracy of each class and overall accuracy of the classification (Kuhn, 2019). The accuracy of each class was defined as the ratio of the number of seedlings correctly classified to each DAE class to the total number of actual samples (seedlings) in each DAE class. The overall accuracy was defined as the ratio of the number of correctly classified seedlings in all DAE classes to the total number of actual seedlings in all DAE classes. An additional metric, i.e., 3-day accuracy, was also defined to study the potential of UAV imagery for predicting the DAE within a 3-day window. The 3-day accuracy was the ratio of the number of samples predicted one day before and one day after the actual DAE (-1 to +1 DAE) to the total number of actual samples in each DAE class. To clarify, 1-day accuracy in DAE means that the predicted DAE was the same as the actual DAE, while 3-day accuracy in DAE means that the predicted DAE was within a 3-day window centered on the actual DAE.

The importance of the image features to the DAE prediction was evaluated using the mean decrease in the Gini index (Belgiu and Drăguţ, 2016; James et al., 2013). The Gini index is used to measure the variance impurity (purity), i.e., the variance of a distribution associated with each class, where a small value implies that a node has observations predominantly from a single class (James et al., 2013). The mean decrease in Gini index was defined as the ratio of the total decrease in Gini index from all the nodes when the feature was used to the number of trees used (James et al., 2013). A large value in the mean decrease in Gini index implied an important feature. This approach was used in this study to identify the important features in predicting DAE. An analysis of variance (ANOVA) test (Sawyer, 2009) at a

0.05 significance level ($\alpha = 0.05$) was performed to determine the significance of the difference between the DAEs of the two top-ranked features identified at earlier imaging dates (first and second weeks of emergence). When the ANOVA showed a significant result, a pairwise comparison known as Tukey's honestly significant difference (HSD, $\alpha = 0.05$) test (Abdi and Williams, 2010) was computed to compare the feature mean difference between DAEs. The statistical analysis was performed using the *aov* and *TukeyHSD* functions in RStudio.

Results and Discussion

Ground Sampling Distance

The ground sampling distance (GSD) was different in each image due to the variation of actual flight heights. Although the UAV was set to fly at a nominal height of 5.0 m, the actual height varied based on the launch location of the UAV and the field slope. The computed GSD ranged from 0.55 to 1.54 mm pixel^{-1} in different plots for UAV images captured on different days. Figure 4 shows images taken on 26 April for two plots with the lowest (0.55 mm pixel^{-1}) and highest (0.94 mm pixel^{-1}) computed GSD. The small plants at DAE 1 and 2 were detectable using the described image processing workflow. This result supports the conclusion that a range of GSD from 0.55 to 0.94 mm pixel^{-1} can be used to detect corn at DAE 1 and 2.

Classification Accuracy for Each Image Date

The classification accuracies of the RF model using data from different imaging dates are shown in figure 5. The number in each grid square indicates the ratio between the predicted number of samples for each DAE and the actual number of samples for the DAE, with darker blue color indicating a higher ratio. Diagonal grid squares show the classification accuracy for each DAE, while the row of squares at the bottom of each grid indicates the 3-day accuracy. As shown in figure 5a, during the first week of emergence, approximately half of the samples were predicted correctly for all DAE classes. The classification accuracy ranged from 0.45 to 0.56, with the exception of DAE 5, which had an accuracy of only 0.20. Figure 5a also shows that 36% of DAE 1 plants were predicted as DAE 2 plants, and more than 20% of DAE 2 plants were predicted as either DAE 1 or DAE 3 plants.

Figure 6 show representative plants for each DAE to illustrate potential reasons for the low classification accuracy. It can be seen that plants for both DAE 1 and DAE 2 could be described as "through surface" or "spike" (Poncet et al., 2019), having similar size and shape. The similarity in size and shape of newly-emerged plants may have caused the misclassification of plants between DAE 1 and DAE 2. In contrast, plants in DAE 3 could be described as having their first leaf open, which increases the distinction in size and shape compared to DAE 1 and DAE 2 and might be a reason for the slightly improved accuracy for DAE 3 (56%). Another possible reason for the low accuracy was that some of the plants in DAE 3 were in the transition stage from spike to first leaf, causing 30% of the plants in DAE 3 to be predicted as DAE 2. Similar results were shown for DAE 4 (about 50% of the samples were predicted as DAE 2 and DAE 3) and for DAE 5 (80% of the samples were predicted as DAE 4), for which the second leaf was becoming visible but the plant size and shape were similar in both DAEs.

Figure 5b shows the classification accuracy for the second week of emergence (DAE 5 to DAE 12). Less than half of the samples for all DAE classes were predicted correctly, with accuracy ranging from 0.21 to 0.43. About 30% of DAE 5 plants were predicted as DAE 7 and DAE 8, which had two leaves open (fig. 6). The low classification accuracy might be due to the lack of distinctive features for some plants transitioning from one leaf to two leaves, i.e., some DAE 5 plants may have transitioned to two-leaf plants. Similarly, about 75% of DAE 7 plants were predicted to have emerged earlier. The prediction for 1-day DAE was best from DAE 8 through DAE 10, but still not better than about

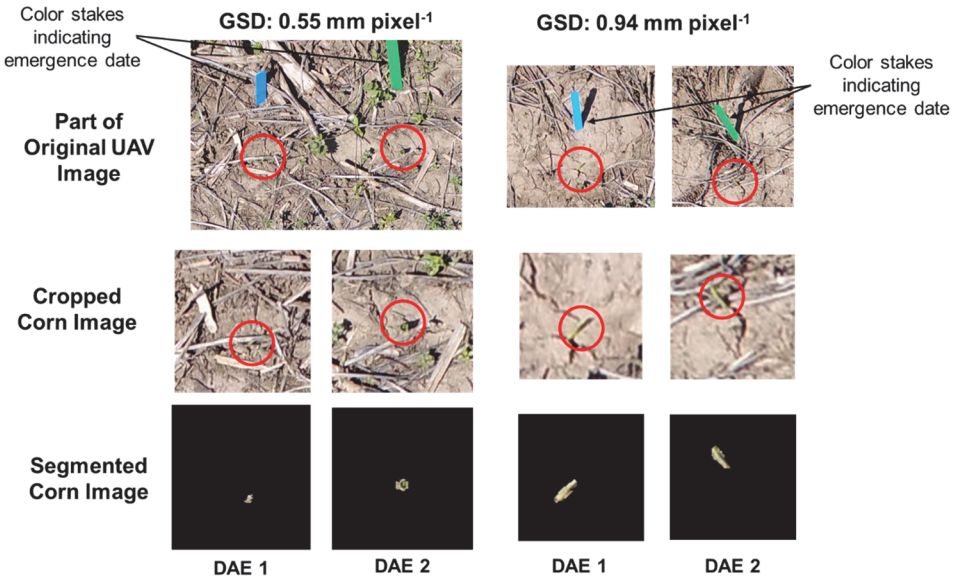

Figure 4. UAV images captured on 26 April at two computed ground sampling distances (GSD). Blue and green color stakes indicate emergence dates of 26 April (DAE 1) and 25 April (DAE 2), respectively.

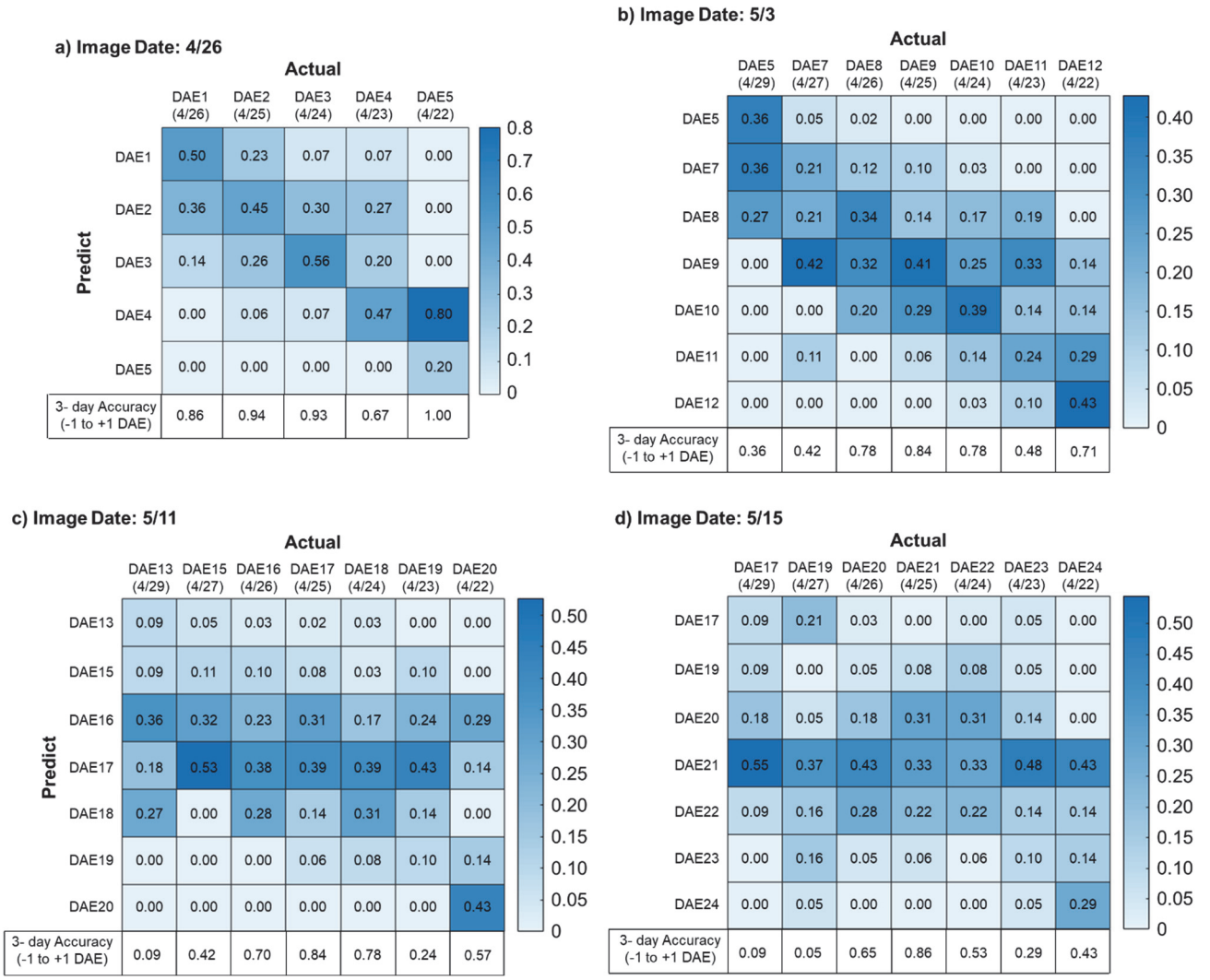

Figure 5. Heat maps of classification accuracy and 3-day accuracy (-1 to +1 DAE) of each DAE class on each imaging date (emergence dates are shown in parentheses).

40%. There was a combination of over- and under-prediction for these DAEs that could be due to the similar plant characteristics during these days, with two open leaves and no substantial differences (fig. 6). Meanwhile, both DAE 11 and DAE 12 had the third leaf visible (fig. 6), which could have improved the classification (the highest classification accuracy was 0.43 for DAE 12 among the other DAEs). However, more than half of these plants were classified as earlier DAEs because they were transitioning from two leaves to three leaves.

The accuracy of predicting 1-day DAE for the third and fourth imaging dates (figs. 5c and 5d; 11 and 15 May) was generally worse than for the earlier imaging dates, ranging from 0.00 to 0.43 accuracy. The poor classification accuracy for these DAEs might be due to emergence of the third leaf and its expansion over a three- to four-day window (DAE 15 to 19 in fig. 6) with an insignificant increase in size. Although the third leaf provides additional features for image analysis, the fact that its emergence and expansion occur over about four to five days diminishes the ability of nadir-view images to accurately classify DAE. Similarly, the fourth leaf emerged and expanded over many days (DAE 20 to 24 in fig. 6), which confounded the 1-day DAE prediction. Additionally, at the fourth leaf stage, older leaves on the lower parts of the plants were blocked by newer leaves, which caused the image features to be less sensitive for differentiating plants at different DAEs. In general, these results support that 1-day DAE prediction is best for emergence through the two-leaf stage; after that, the sensitivity in predicting DAE classes is reduced.

Another reason for DAE misclassification was the limited number of plants evaluated. The total number of plants that emerged from 22 to 29 April was 627. The plant number ranged from 120 to 170 for emergence dates 24 to 26 April but was less than 70 for the other dates. The small datasets for training and testing potentially skewed the model sensitivity (O'Brien and Ishwaran, 2019). Additionally, although the camera was adjusted to obtain nadir images, seedlings that were not at the centers of images had a somewhat oblique view, resulting in errors due to image distortion (Seifert et al., 2019).

Occasionally, the emergence and growth of seedlings may not be uniform due to varying soil and residue conditions, which caused some variability in the image features

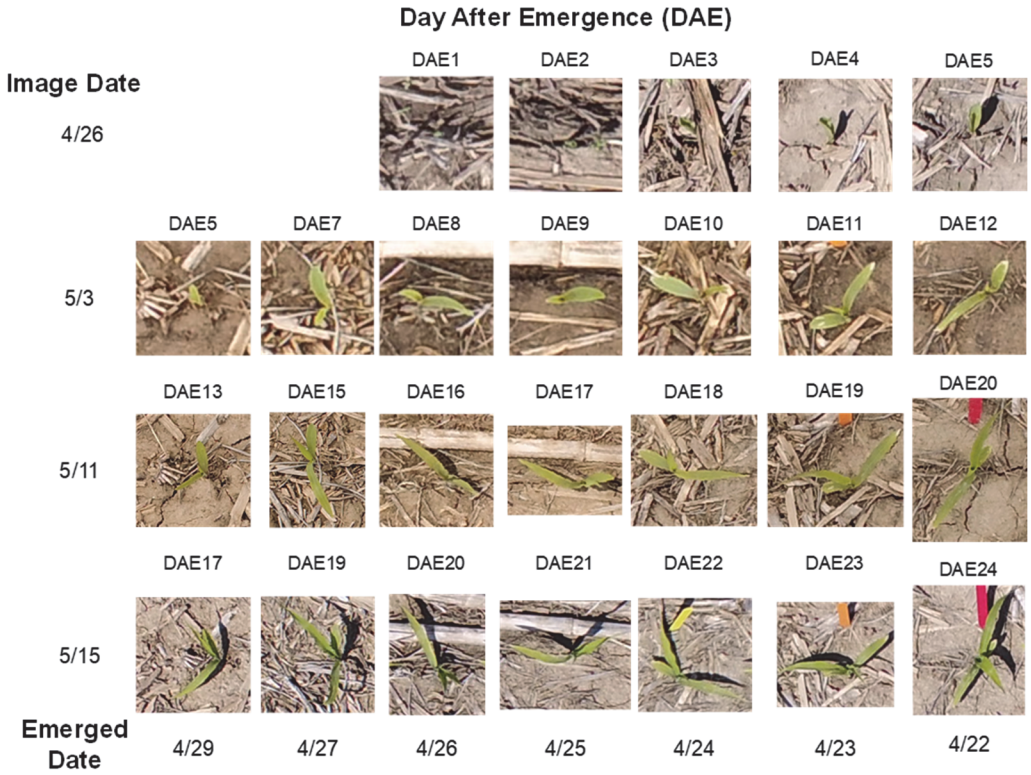

Figure 6. Example cropped corn images from UAV images of different DAE on each imaging date.

from plant to plant. One of the most vital factors affecting corn emergence and seedling growth in the first six weeks is soil temperature (Alessi and Power, 1971). Studies showed that lower soil temperature caused by residue from no-till (similar to the field in our study) delayed corn emergence, early growth, and development (Al-Darby and Lowery, 1987; Bollero et al., 1996). Figures 7a and 7b show two examples of residue distribution and its influence on growth rate for plants that emerged on the same day (DAE 5). In figure 7a, a DAE 5 plant was classified correctly with the common feature of the second visible leaf (fig. 6). In contrast, figure 7b also shows a DAE 5 plant, but this plant was growing in low-residue conditions and was misclassified as DAE 7. The low-residue conditions enabled higher soil temperature (i.e., darker soil absorbed more sunlight) and more rapid growth. Figure 7c and 7d show another example of image feature variability caused by the orientation of the coleoptile (a protective sheath covering the first leaf). In figure 7c, a DAE 1 plant was classified correctly with the coleoptile emerging vertically from the soil surface. In figure 7d, the coleoptile did not emerge vertically from the soil surface but instead was forced to grow horizontally as it encountered surface residue, and the plant was misclassified as DAE 2.

Three-Day Classification Accuracy for Each Image Date and Overall Accuracy

During the first week of emergence, the 3-day accuracy was high for each DAE (>0.85) except for DAE 4 (0.67) (fig. 5a). For the second imaging date (fig. 5b), the 3-day accuracy was not as good as the first week, but still ranged from 0.36 to 0.84, with no consistent trend from day to day. Similar results were indicated for the last two imaging dates (figs. 5c and 5d). Figure 8 shows the overall prediction accuracies of the 1-day DAE and 3-day DAE for each imaging date. On average, UAV imagery predicted the 1-day DAE with moderate overall accuracy (i.e., <0.5), but the accuracy greatly improved when the performance measure for DAE was expanded to a 3-day window. As with predicting 1-day DAE, the DAE classification sensitivity using the 3-day window was reduced as the plants matured. Prediction of plant emergence in a 3-day period is useful for studies on corn emergence uniformity. Previous studies on the effects

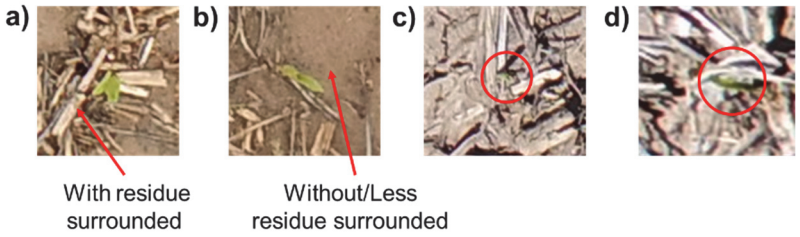

Figure 7. Example images of correctly classified and misclassified plants: (a) correctly classified DAE 5 plant surrounded by average residue for the field, (b) DAE 5 plant misclassified as DAE 7 plant surrounded by less residue, (c) correctly classified DAE 1 plant with coleoptile emerging vertically from soil surface (red circle), and (d) DAE 1 plant misclassified as DAE 2 plant with coleoptile growing horizontally (red circle).

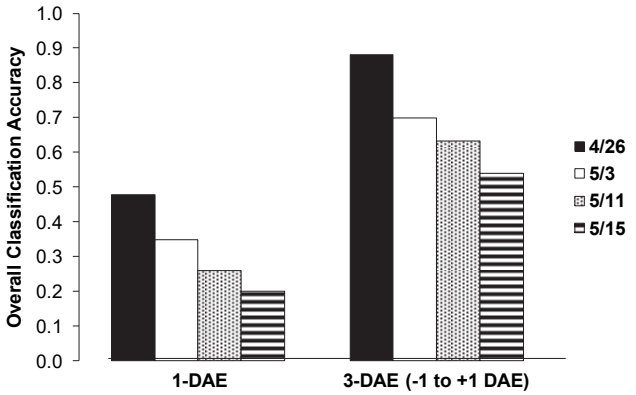

Figure 8. Overall accuracies of exact DAE and DAE within a three-day window for each imaging date.

of delayed emergence on yield used wider ranges, such as one to three weeks (Andrade and Abbate, 2005; Liu et al., 2004; Nafziger et al., 1991). Only one study investigated the effects of delayed planting of 2, 5, 8, and 12 days on yield (Lawles et al., 2012). Moreover, indication of delay was based on delayed planting days without documenting the exact emergence day. This might be due to the time-consuming and labor-intensive field work needed to record the exact emergence day. Therefore, the present study shows proof-of-concept for using high-resolution UAV images for predicting DAE within a 3-day period. Additional automation of data processing would be needed to extend the scale of this process.

Identification of Important Image Features

It is useful to evaluate the importance of different image features on the performance of DAE estimation. Figure 9 shows the variable importance of the important features determined using the mean decrease in Gini index. Two features, i.e., area and SF2 (ratio of major axis length to area) were consistently among the top five features for all imaging dates, and diameter was among the top three features for all dates. The fact that these three features were consistently strong contributors for predicting DAE suggests their importance, and therefore they should be the focus of future studies.

Figure 10 illustrates the mean diameter and area for the first two imaging dates (26 April and 3 May) at different DAEs. The diameter and area increased with increasing DAE, which corresponded to the plant growth with increasing leaf size and additional visible leaves. These morphological features captured through UAV images, provide

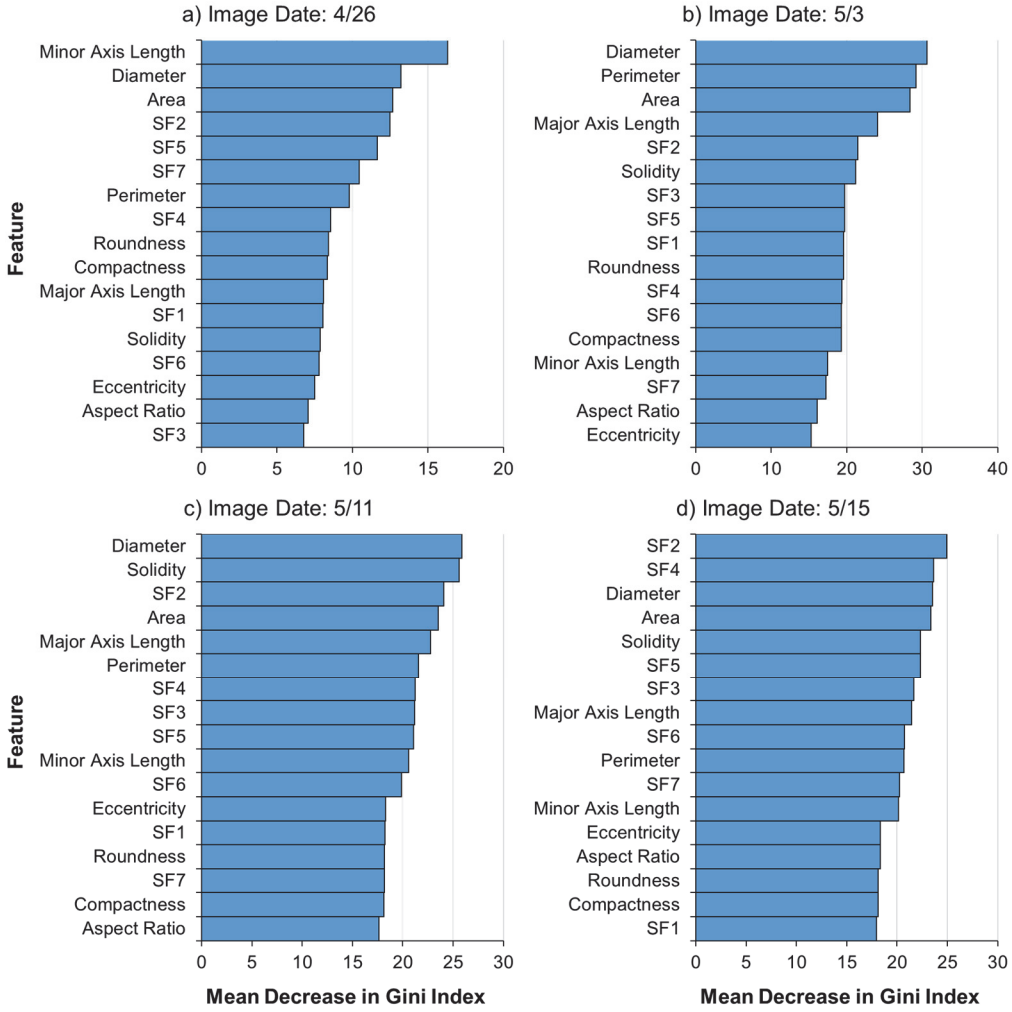

Figure 9. Variable importance of important features based on mean decrease in Gini index for four imaging dates.

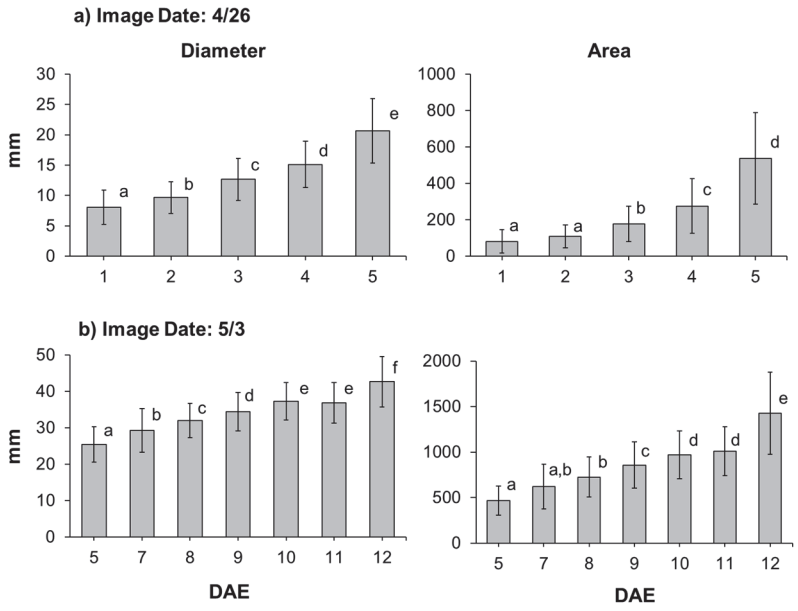

Figure 10. Mean diameter and area for the first two imaging dates (26 April and 3 May) at different DAE. In each chart, bars with different letters are significantly different in the mean at $p < 0.05$ for the Tukey HSD test.

phenological information that may be useful for crop growth modeling (Dodig et al., 2019; Wang et al., 2018). Interestingly, minor axis length ranked as the most important feature for the first imaging date but was much less important for the subsequent imaging dates.

Figure 11 shows the minor and major axis lengths of the ellipse region of corn plants at different DAEs. During the first week of emergence (fig. 11a), the ellipse region covered the complete area of the first leaf. Thus, the minor axis length increased with increasing leaf size. In contrast, for the second week onward (figs. 11b to 11d), the ellipse region was the overall nadir view of the plant, in which the minor axis length could represent the width of one leaf or the center of the plant (at the whorl or near it, fig. 11d). This uncertainty caused inconsistent trends in this feature at different DAEs.

Future Study and Applications

This study provided meaningful estimates of post-emergence DAE using UAV images. To achieve this, it was necessary to fly the imaging system at a low altitude (~5 m) to acquire sufficient GSD, which required a higher-resolution camera to achieve the equivalent GSD with a larger area per scene. In addition, manual identification of corn plants was required because of the presence of winter annual weeds growing alongside the emerging corn plants. Plant residues from the previous growing season also added a challenge to the image processing for predicting DAE. However, because conservation and no-till systems are often encouraged for soil conservation and health, this issue needs to be resolved. Future work should include more advanced image processing or deep learning (DL) models to automate the

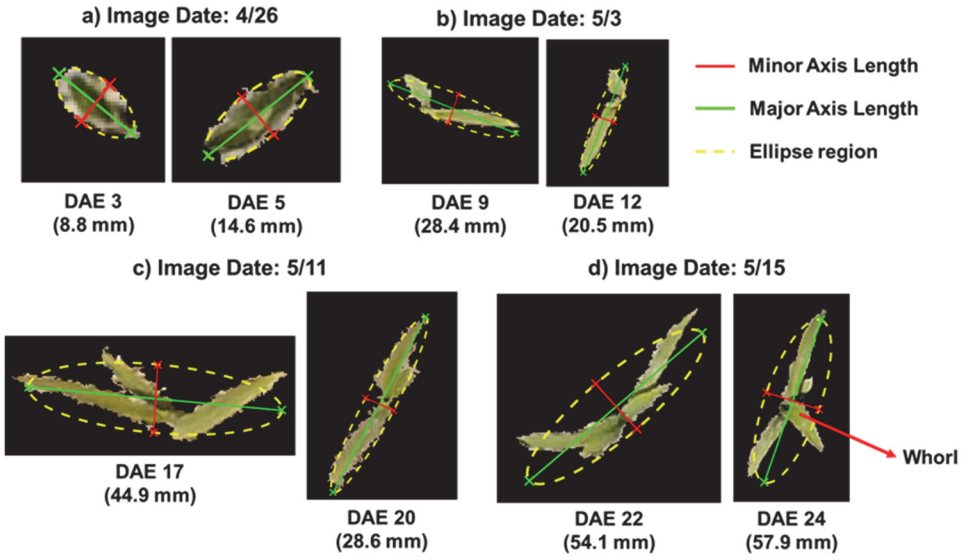

Figure 11. Minor and major axes of corn plants at different DAE on four imaging dates (values in parentheses are minor axis lengths).

background removal (weeds and residues), such as using DL models to detect and segment single plants from each image.

As automation of image processing is further refined, the time and labor needed for collecting field-scale UAV imagery for this type of analysis will become more reasonable. As a bridge to that goal, more large-scale field experiments on emergence uniformity evaluation using UAV images should be conducted. These studies might include other soil and crop management factors, such as investigating the effects of emergence uniformity due to different tillage systems (Lithourgidis et al., 2005), planting depths (Hussen et al., 2013; Molatudi and Mariga, 2009), and seed sizes (Molatudi and Mariga, 2009). In addition, plant morphological features may be affected by environmental factors including soil and weather conditions, which may cause bias of DAE estimation using only image features. Therefore, in future work, the DAE estimation model should also include environmental information such as growing degree day (GDD), soil apparent electricity conductivity (EC_a), and soil information from a real-time planting sensor (SmartFirmer, Precision Planting, Tremont, Ill.).

To improve the classification accuracy, different approaches to UAV data collection could be tested. For example, collecting a sequence of multiple images with varying sufficient overlaps, such as 85% front and 70% side overlaps for field-scale experiments as suggested by aerial image stitching software (Pix4D Inc., Denver, Colo.), to produce an orthomosaic (Lin and Medioni, 2007) will reduce the variability of image features caused by imaging plants at oblique angles. In addition, orthomosaic generation can be useful for mapping emergence uniformity for the entire field and the proportion of early and delayed emergence. This would be beneficial in making replanting decisions (Nafziger et al., 1991). Another UAV data collection approach could be collecting a series of nadir and oblique (camera adjusted to vertical angles of 45° and 135°) images to generate 3D dense point clouds (Che et al., 2020; Karpina et al., 2016; Zhou et al., 2018). These 3D dense point clouds may be useful for extracting other features, such as plant height and total number of leaves.

Conclusion

This research demonstrated that UAV imagery can be used to detect newly-emerged corn plants and estimate emergence dates, which will be valuable for evaluating plant emergence uniformity and replanting decisions. The required GSD to detect the small corn seedlings (DAE 1 to 5) during the first week after emergence ranged from 0.55 to 0.94 mm $pixel^{-1}$. UAV imagery was not able to predict the 1-day DAE with high overall accuracies, but was capable of predicting DAE within a 3-day window (-1 to +1 DAE) with higher overall accuracies. DAE prediction was best for the first two weeks after emergence (from emergence through two-leaf stage). Afterward, sensitivity in predicting DAE was reduced. Diameter, area, and SF2 (i.e., minor axis length/area) were important features identified for differentiating DAE for all imaging dates, with an additional feature (minor axis length) for the first week of emergence. Further studies should acquire multiple images and generate an orthomosaic to reduce image feature variability. More plant samples at each DAE should be included to obtain a more robust model and subsequently increase the actual DAE prediction accuracy. Furthermore, additional environmental data should be included in the prediction model to reduce the DAE estimation bias.

To conclude, this study serves as the first approach to estimating corn emergence date in field conditions using UAV imagery with a high overall 3-day estimation accuracy. The methods and results of this study may provide baseline information for researchers who will conduct similar projects in the future.

Acknowledgements

We would like to thank Lance Conway, Research Specialist in the College of Agriculture, Food, and Natural Resources at the University of Missouri, for his assistance in preparing the experiment site. We also thank the members of the Precision and Automated Agriculture Lab at the University of Missouri, including Dandan Fu, Jianjun Yin, Jing Zhou, and Aijing Feng, for their assistance in UAV data collection. This research was partially funded by the USDA Agricultural Research Service (Project 5070-12610-005).

References

Abdi, H., & Williams, L. J. (2010). Tukey's honestly significant difference (HSD) test. *Encyclopedia Res. Design, 3*(1), 583-585. https://doi.org/10.4135/9781412961288.n181

Al-Darby, A. M., & Lowery, B. (1987). Seed zone soil temperature and early corn growth with three conservation tillage systems. *SSSA J., 51*(3), 768-774. https://doi.org/10.2136/sssaj1987.03615995005100030035x

Alessi, J., & Power, J. F. (1971). Corn emergence in relation to soil temperature and seeding depth. *Agron. J., 63*(5), 717-719. https://doi.org/10.2134/agronj1971.00021962006300050018x

Andrade, F. H., & Abbate, P. E. (2005). Response of maize and soybean to variability in stand uniformity. *Agron. J., 97*(4), 1263-1269. https://doi.org/10.2134/agronj2005.0006

Belgiu, M., & Drăguţ, L. (2016). Random forest in remote sensing: A review of applications and future directions. *ISPRS J. Photogram. Remote Sens., 114*, 24-31. https://doi.org/10.1016/j.isprsjprs.2016.01.011

Bollero, G. A., Bullock, D. G., & Hollinger, S. E. (1996). Soil temperature and planting date effects on corn yield, leaf area, and plant development. *Agron. J., 88*(3), 385-390. https://doi.org/10.2134/agronj1996.00021962008800030005x

Breiman, L., & Cutler, A. (2018). Breiman and Cutler's random forests for classification and regression. Retrieved from https://cran.r-project.org/web/packages/randomForest/randomForest.pdf

Chandpa, K. R., Jani, A. M., & Prajapati, G. I. (2014). Comparative study of linear and non-linear contrast enhancement techniques. *Intl. J. Res. Sci. Innov., 1*(6), 37-41.

Chaugule, A., & Mali, S. N. (2014). Evaluation of texture and shape features for classification of four paddy varieties. *J. Eng., 2014*, article 617263. https://doi.org/10.1155/2014/617263

Che, Y., Wang, Q., Xie, Z., Zhou, L., Li, S., Hui, F., ... Ma, Y. (2020). Estimation of maize plant height and leaf area index dynamics using an unmanned aerial vehicle with oblique and nadir photography. *Ann. Bot., 126*(4), 765-773. https://doi.org/10.1093/aob/mcaa097

Chen, X., Xun, Y., Li, W., & Zhang, J. (2010). Combining discriminant analysis and neural networks for corn variety identification. *Comput. Electron. Agric., 71*, S48-S53. https://doi.org/10.1016/j.compag.2009.09.003

Dodig, D., Božinović, S., Nikolić, A., Zorić, M., Vančetović, J., Ignjatović-Micić, D., ... Altmann, T. (2019). Image-derived traits related to mid-season growth performance of maize under nitrogen and water stress. *Front. Plant Sci., 10*, article 814. https://doi.org/10.3389/fpls.2019.00814

FAO. (2020). FAOSTAT statistical database. Rome, Italy: United Nations FAO. Retrieved from http://www.fao.org/faostat/en/#data/QC/visualize

Gnädinger, F., & Schmidhalter, U. (2017). Digital counts of maize plants by unmanned aerial vehicles (UAVs). *Remote Sensing, 9*(6), article 544. https://doi.org/10.3390/rs9060544

Hussen, S., Alemu, B., & Ahmed, F. (2013). Effect of planting depth on growth performance of maize (*Zea mays*) at the experimental site of Wollo University, Dessie, Ethiopia. *Intl. J. Sci. Basic Appl. Res., 8*(1), 10-15.

James, G., Witten, D., Hastie, T., & Tibshirani, R. (2013). *An introduction to statistical learning*. New York, NY: Springer. https://doi.org/10.1007/978-1-4614-7138-7

Jin, X., Liu, S., Baret, F., Hemerlé, M., & Comar, A. (2017). Estimates of plant density of wheat crops at emergence from very low altitude UAV imagery. *Remote Sens. Environ., 198*, 105-114. https://doi.org/10.1016/j.rse.2017.06.007

Karpina, M., Jarząbek-Rychard, M., Tymków, P., & Borkowski, A. (2016). UAV-based automatic tree growth measurement for biomass estimation. *Intl. Arch. Photogram. Remote Sens. Spat. Info. Sci., 8*, 685-688. https://doi.org/10.5194/isprs-archives-XLI-B8-685-2016

Klopfenstein, T. J., Erickson, G. E., & Berger, L. L. (2013). Maize is a critically important source of food, feed, energy, and forage in the USA. *Field Crops Res., 153*, 5-11. https://doi.org/10.1016/j.fcr.2012.11.006

Kuhn, M. (2019). Package 'caret': RStudio. Retrieved from https://cran.r-project.org/web/packages/caret/caret.pdf

Lauer, J. G. (1997). Corn replant/late-plant decisions in Wisconsin. Madison, WI: University of Wisconsin Cooperative Extension.

Lawles, K., Raun, W., Desta, K., & Freeman, K. (2012). Effect of delayed emergence on corn grain yields. *J. Plant Nutr., 35*(3), 480-496. https://doi.org/10.1080/01904167.2012.639926

Lillesand, T., Kiefer, R. W., & Chipman, J. (2004). *Remote sensing and image interpretation* (5th Ed.). Hoboken, NJ: John Wiley & Sons.

Lin, Y., & Medioni, G. (2007). Map-enhanced UAV image sequence registration and synchronization of multiple image sequences. *Proc. IEEE Conf. Computer Vision and Pattern Recognition*. Piscataway, NJ: IEEE. https://doi.org/10.1109/CVPR.2007.383428

Lithourgidis, A. S., Tsatsarelis, C. A., & Dhima, K. V. (2005). Tillage effects on corn emergence, silage yield, and labor and fuel inputs in double cropping with wheat. *Crop Sci., 45*(6), 2523-2528. https://doi.org/10.2135/cropsci2005.0141

Liu, W., Tollenaar, M., Stewart, G., & Deen, W. (2004). Response of corn grain yield to spatial and temporal variability in emergence. *Crop Sci., 44*(3), 847-854. https://doi.org/10.2135/cropsci2004.8470

Molatudi, R., & Mariga, I. (2009). The effect of maize seed size and depth of planting on seedling emergence and seedling vigour. *J. Appl. Sci. Res., 5*(12), 2234-2237.

Nafziger, E. D., Carter, P. R., & Graham, E. E. (1991). Response of corn to uneven emergence. *Crop Sci., 31*(3), 811-815. https://doi.org/10.2135/cropsci1991.0011183X003100030053x

Najafabadi, S. S. M., & Farahani, L. (2012). Shape analysis of common bean (*Phaseolus vulgaris* L.) seeds using image analysis. *Intl. Res. J. Appl. Basic Sci., 3*(8), 1619-1623.

O'Brien, R., & Ishwaran, H. (2019). A random forest quantile classifier for class imbalanced data. *Pattern Recog., 90*, 232-249. https://doi.org/10.1016/j.patcog.2019.01.036

Orych, A. (2015). Review of methods for determining the spatial resolution of UAV sensors. *Intl. Arch. Photogram. Remote Sens. Spat. Info. Sci., XL-1/W4*, 391-395. https://doi.org/10.5194/isprsarchives-XL-1-W4-391-2015

Oshiro, T. M., Perez, P. S., & Baranauskas, J. A. (2012). How many trees in a random forest? *Proc. Intl. Workshop on Machine Learning and Data Mining in Pattern Recognition* (pp. 154-168). New York, NY: Springer. https://doi.org/10.1007/978-3-642-31537-4_13

Poncet, A. M., Fulton, J. P., McDonald, T. P., Knappenberger, T., & Shaw, J. N. (2019). Corn emergence and yield response to row-unit depth and downforce for varying field conditions. *Appl. Eng. Agric., 35*(3), 399-408. https://doi.org/10.13031/aea.12408

Ransom, J., Berglund, D. R., Endres, G. J., & McWilliams, D. A. (2020). Corn growth and management quick guide. Fargo, ND: North Dakota State University Extension Service. Retrieved from https://www.ag.ndsu.edu/publications/crops/corn-growth-and-management-quick-guide/a1173.pdf

Rodriguez-Galiano, V. F., Ghimire, B., Rogan, J., Chica-Olmo, M., & Rigol-Sanchez, J. P. (2012). An assessment of the effectiveness of a random forest classifier for land-cover classification. *ISPRS J. Photogram. Remote Sens., 67*, 93-104. https://doi.org/10.1016/j.isprsjprs.2011.11.002

Sawyer, S. F. (2009). Analysis of variance: The fundamental concepts. *J. Manual Manip. Therapy, 17*(2), 27E-38E. https://doi.org/10.1179/jmt.2009.17.2.27E

Seifert, E., Seifert, S., Vogt, H., Drew, D., van Aardt, J., Kunneke, A., & Seifert, T. (2019). Influence of drone altitude, image overlap, and optical sensor resolution on multi-view reconstruction of forest images. *Remote Sensing, 11*(10), 1252. https://doi.org/10.3390/rs11101252

Shiferaw, B., Prasanna, B. M., Hellin, J., & Bänziger, M. (2011). Crops that feed the world: 6. Past successes and future challenges to the role played by maize in global food security. *Food Security, 3*(3), article 307. https://doi.org/10.1007/s12571-011-0140-5

Shuai, G., Martinez-Feria, R. A., Zhang, J., Li, S., Price, R., & Basso, B. (2019). Capturing maize stand heterogeneity across yield-stability zones using unmanned aerial vehicles (UAV). *Sensors, 19*(20), 4446. https://doi.org/10.3390/s19204446

Varela, S., Dhodda, P. R., Hsu, W. H., Prasad, P. V., Assefa, Y., Peralta, N. R., ... Ciampitti, I. A. (2018). Early-season stand count determination in corn via integration of imagery from unmanned aerial systems (UAS) and supervised learning techniques. *Remote Sensing, 10*(2), 343. https://doi.org/10.3390/rs10020343

Wang, N., Wang, E., Wang, J., Zhang, J., Zheng, B., Huang, Y., & Tan, M. (2018). Modeling maize phenology, biomass growth, and yield under contrasting temperature conditions. *Agric. Forest Meteorol., 250-251*, 319-329. https://doi.org/10.1016/j.agrformet.2018.01.005

Zhang, J., Basso, B., Price, R. F., Putman, G., & Shuai, G. (2018). Estimating plant distance in maize using unmanned aerial vehicle (UAV). *PLoS One, 13*(4), e0195223. https://doi.org/10.1371/journal.pone.0195223

Zhou, J., Fu, X., Schumacher, L., & Zhou, J. (2018). Evaluating geometric measurement accuracy based on 3D reconstruction of automated imagery in a greenhouse. *Sensors, 18*(7), 2270. https://doi.org/10.3390/s18072270